

Modelling the deformation of face centred cubic crystals to study the effect of slip on $\{110\}$ planes

G Sarma, B Radhakrishnan and T Zacharia

Computer Science and Mathematics Division, Oak Ridge National Laboratory, Oak Ridge,
TN 37831-6359, USA

Received 4 August 1999

Abstract. The deformations of single crystals and polycrystals of aluminium have been modelled using the finite-element method. The constitutive behaviour is modelled using crystal plasticity to account for the plastic deformation by slip, and to track the hardening and reorientation of the material. By discretizing each crystal with a large number of elements, the non-uniform deformations due to local inhomogeneities and interactions with neighbouring crystals are modelled. Simulations of plane strain compression of (001)[110] oriented single crystals are used to demonstrate the ability of the model to capture shearing in the rolling-normal plane, and the consequent reorientation of the crystal to the $\{112\}\langle 111\rangle$ copper components. The simulations are used to examine the effect of including $\{110\}\langle 110\rangle$ slip systems in addition to the usual $\{111\}\langle 110\rangle$ systems for face centred cubic metals on the stability of the cubic orientation. The results indicate that slip on $\{110\}$ planes greatly enhances the stability of the cubic orientation, while having little contribution in the deformation of most other orientations.

1. Introduction

Deformation processing is an important component in the manufacturing of metal products. The changes in texture and microstructure that accompany the deformation process control the material behaviour during subsequent thermomechanical processing. Understanding and predicting the texture and microstructure evolution during processing of metals remains a subject for extensive research. In this regard, the merging of the finite-element method (FEM) as a numerical tool for solving the boundary value problem associated with material motion with crystal plasticity theory as a constitutive description for plastic deformation by slip has developed into a significant modelling capability. Early efforts in this area utilized crystal plasticity as a state variable theory in place of simpler continuum models in finite-element simulations of industrial metal working operations such as rolling, forging, extrusion, etc (e.g. Mathur and Dawson 1989, Mathur *et al* 1990, Kalidindi *et al* 1992, Beaudoin *et al* 1994). Some recent efforts at combining FEM and crystal plasticity to model deformation processing of metals have focused at the mesoscale, by shifting the domain used for discretization from the entire workpiece to a single polycrystalline aggregate. These simulations are aimed at using the modelling capabilities to gain better insights into the role of grain interactions on the non-uniform deformations of metal polycrystals. While some early efforts in this area were restricted to two-dimensional (2D) domains (e.g. Becker 1991, Anand and Kalidindi 1994, Becker and Panchanadeswaran 1995), more recent efforts have been able to treat fairly large three-dimensional (3D) meshes by taking advantage of parallel computing resources (Beaudoin *et al* 1996, Sarma *et al* 1998b, Mika and Dawson 1998).

Applications of FEM and crystal plasticity to deformation process modelling at the mesoscale proceed by discretizing each grain of a polycrystal with a large number of elements, so that the non-uniform deformations of individual grains can be modelled. Unlike in continuum models, where grains are merely abstract entities with no physical description associated with them, here the grains and their neighbours are explicitly defined by the finite-element model. This feature enables the model to incorporate effects of neighbour interactions on the inhomogeneous deformations of individual grains, and the effect of such inhomogeneities on the texture and microstructure evolution. Additionally, these simulations can provide quantitative information on the distribution of orientations and stored energy in the deformed microstructure, which provides a means to simulate the texture and microstructure evolution during recovery and recrystallization (Radhakrishnan *et al* 1998a, b).

The objective of the work described in this paper is to apply the mesoscale deformation modelling approach to single crystals and polycrystals of aluminium deformed in plane strain compression to study their non-uniform deformations. First, some results are presented on modelling the plane strain compression of a single crystal with initial orientation (001)[110]. This particular orientation has been studied extensively, both experimentally and through modelling (Butler and Hu 1989, Becker *et al* 1991, Akef and Driver 1991, Cizek *et al* 1996) and serves as a good test case to validate the mesoscale modelling approach. It is shown that the results are quite consistent with experimental observations, in terms of changes in both orientation and geometry. These simulations are also used to illustrate that use of 2D models may not always be adequate for plane strain deformations.

As a novel application of the mesoscale modelling approach, simulations have been carried out to examine the effect of slip on $\{110\}\langle 110 \rangle$ systems on the stability of the cubic orientation, which is an important component in textures produced during hot rolling and also in recrystallized microstructures. Optimization of cubic texture is one of the key issues in the hot rolling of commercial aluminium alloys for beverage-can applications. Subsequent cold rolling of the hot-band is designed to provide, in addition to the required mechanical properties, an optimum combination of cubic and other deformation components that can minimize material waste due to earing. Therefore, considerable effort has been made in the past to understand texture evolution during thermomechanical processing of aluminium alloys. It is well known that plastic deformation in face centred cubic (fcc) metals is accommodated by shearing of $\{111\}$ planes in $\langle 110 \rangle$ directions. This knowledge has been utilized extensively in the application of crystal plasticity models to study the texture development during cold working of aluminium and its alloys. It has been postulated that when aluminium is deformed at elevated temperatures, slip occurs on other planes, notably the $\{100\}$, $\{110\}$ and $\{112\}$ (Bacroix and Jonas 1988, Maurice and Driver 1997a). Slip activity on the non-octahedral systems alters the relative strength of various texture components during deformation in plane strain compression. In particular, the $\{011\}\langle 211 \rangle$ brass component is enhanced by slip on the $\{112\}$ planes, and the $\{001\}\langle 100 \rangle$ cubic component is stabilized by slip on $\{110\}$ planes.

Previous efforts on modelling the effect of slip on the $\{110\}$ planes (Bacroix and Jonas 1988, Maurice and Driver 1993, 1997b, Raabe 1995) have been through analytical models based on some simplifying assumptions or through numerical simulations using an aggregate of grains. Simulations with an aggregate of grains have relied on various assumptions to partition the deformation among the individual grains, such as the full constraints Taylor model (Taylor 1938), the relaxed constraints model (Honneff and Mecking 1978) or the self-consistent model (Lebensohn and Tomé 1993, Molinari and Tóth 1994). This approach is not suited for the examination of the heterogeneous deformation of single crystals or individual grains in a polycrystal, since they assume the deformation of each grain to be homogeneous. The modelling work described in this paper is believed to be the first attempt at simulating the

deformation of single crystals in three dimensions using the FEM. No assumptions regarding the partitioning of deformation among the grains are required. Due to the use of a rate-dependent constitutive model, assumptions are also not needed regarding the choice of active slip systems.

In addition to single crystals initially at and near the cubic orientation, deformations of polycrystals containing cubic grains have been simulated to study the effect of constraints from neighbours. Unlike experiments with polycrystals, where it may be difficult to monitor the behaviour of interior grains during deformation, the mesoscale modelling approach provides information at all locations in the discretized domain. In this regard, it is possible to examine the effect of neighbour interactions in altering the deformation of a grain from that specified by the boundary conditions. Such deviations from the overall deformation are implicit in the mesoscale finite-element model.

2. Finite-element formulation

The finite-element formulation used for the present study is based on the hybrid formulation described by Beaudoin *et al* (1995). It is assumed that elastic deformations are negligibly small, and that deformation occurs by slip dominated plastic flow of the material. Due to the limited modes of deformation available through slip, the crystal must rotate to accommodate arbitrary deformations. The resulting texture development is modelled using a constitutive law based on crystal plasticity.

Details regarding the constitutive model and the finite-element formulation are described elsewhere (Beaudoin *et al* 1995) and only a brief outline is given here. A viscoplastic constitutive law relates the rate of shearing $\dot{\gamma}^{(\alpha)}$ to the resolved shear stress $\tau^{(\alpha)}$ on each slip system α :

$$\dot{\gamma}^{(\alpha)} = \dot{\gamma}_0 \left| \frac{\tau^{(\alpha)}}{\hat{\tau}} \right|^{1/m} \text{sign}(\tau^{(\alpha)}) \quad (1)$$

where m is the rate sensitivity parameter and $\dot{\gamma}_0$ is a reference rate of shearing. $\hat{\tau}$ is a hardness parameter which represents resistance to plastic deformation due to interactions among dislocations. The symmetric part of the Schmid tensor $\mathbf{P}^{(\alpha)}$ (dyadic product of the slip direction and slip plane normal vectors) relates the crystal deviatoric Cauchy stress $\boldsymbol{\sigma}'_c$ to the resolved shear stress and the rate of deformation \mathbf{D}_c to the shearing rates:

$$\tau^{(\alpha)} = \boldsymbol{\sigma}'_c \cdot \mathbf{P}^{(\alpha)} \quad (2)$$

$$\mathbf{D}_c = \sum_{\alpha} \dot{\gamma}^{(\alpha)} \mathbf{P}^{(\alpha)}. \quad (3)$$

Eliminating $\dot{\gamma}^{(\alpha)}$ between (1) and (3), and substituting (2) for $\tau^{(\alpha)}$ leads to an expression for the crystal deformation rate in terms of the deviatoric stress,

$$\mathbf{D}_c = \left[\sum_{\alpha} \frac{\dot{\gamma}_0}{\hat{\tau}} \left| \frac{\tau^{(\alpha)}}{\hat{\tau}} \right|^{(1/m)-1} \mathbf{P}^{(\alpha)} \otimes \mathbf{P}^{(\alpha)} \right] \boldsymbol{\sigma}'_c = \mathcal{S}_c \boldsymbol{\sigma}'_c \quad (4)$$

where \mathcal{S}_c is the fourth-order crystal 'compliance' tensor. The rate dependence of (1) permits inversion of (4), and the expression of the crystal deviatoric stress under a given deformation rate as

$$\boldsymbol{\sigma}'_c = \mathcal{S}_c^{-1} \mathbf{D}_c. \quad (5)$$

The nonlinear nature of the crystal constitutive equation (5) requires an iterative method to compute the deviatoric stress for a given rate of deformation. The anisotropic response due to the crystal orientation is reflected in the crystal compliance.

The crystal rate of deformation is the symmetric part of the crystal velocity gradient and prescribes the rate of shearing of slip planes. The skew-symmetric part of the crystal velocity gradient W_c controls the rotation of the crystal, and contains contributions from both the spin associated with the plastic flow, and the rigid rotation R^* of the crystal lattice necessary to maintain compatibility with neighbouring crystals. The difference between the applied spin and the plastic spin due to slip provides an expression for the crystal reorientation rate

$$\dot{R}^* = \left(W_c - \sum_{\alpha} \dot{\gamma}^{(\alpha)} Q^{(\alpha)} \right) R^* \quad (6)$$

where $Q^{(\alpha)}$ is the skew-symmetric part of the Schmid tensor.

The plastic deformation of the material is modelled in incremental fashion, by solving the boundary value problem for material motion at each strain increment. Balance laws for equilibrium and mass conservation are applied in conjunction with the constitutive assumptions discussed above. Following the approach of Beaudoin *et al* (1995), a hybrid finite-element formulation is employed for this purpose. Instead of developing the equilibrium statement from the balance of momentum at the global level, here it is written as a balance of tractions at the inter-element boundaries. Weighted residuals are formed on the equilibrium statement and the constitutive relation. A third residual on the conservation of mass (which for the case of incompressible plastic deformation reduces to a divergence-free velocity field) completes the formulation. Interpolation functions are introduced for the nodal velocities, element stress components and the pressure. A proper choice of the shape functions for the stress permits elimination of the stress degrees of freedom at the element level. The result is a system of equations for the discretized velocity field, which is solved assuming fixed material state and geometry.

Upon obtaining a converged velocity solution, the material state and geometry are updated. The material is characterized by the orientation of the crystal and the hardness parameter. The reorientation rate given by (6) is used to update the orientation, while the hardness is evolved using a modified Voce type law,

$$\dot{\hat{\tau}} = H_0 \left(\frac{\hat{\tau}_s - \hat{\tau}}{\hat{\tau}_s - \hat{\tau}_i} \right) \dot{\gamma}^* \quad (7)$$

where hardening rate H_0 and initial hardness $\hat{\tau}_i$ are material parameters. $\dot{\gamma}^*$ is a measure of the net shearing rate on all of the slip systems,

$$\dot{\gamma}^* = \sum_{\alpha} |\dot{\gamma}^{(\alpha)}|. \quad (8)$$

The saturation hardness $\hat{\tau}_s$ based on the current slip system state is given by

$$\hat{\tau}_s = \hat{\tau}_{s_0} \left(\frac{\dot{\gamma}^*}{\dot{\gamma}_s} \right)^{m'} \quad (9)$$

where $\hat{\tau}_{s_0}$, $\dot{\gamma}_s$ and m' are material parameters.

Development of the material response entails solution of the nonlinear crystal constitutive relation for each element, and must be performed during each iteration for the velocity field at a given strain increment. In this respect, the methodology described above proves to be computationally demanding. The use of the hybrid approach leads to the introduction of additional degrees of freedom for the crystal stresses, thereby adding to the computational burden associated with the stiffness calculations. The advantage of using this approach is the smoothness in the stress field, due to the enforcement of traction balance at the element interfaces in an approximate sense (Beaudoin *et al* 1995). In the finite-element context, the numerical integration required for computing the stiffness matrix can be performed

concurrently for all elements. The choice of piecewise discontinuous interpolation functions for the stress is a key feature of the formulation, which enables computation of the stiffness matrices in concurrent fashion for all elements. In turn, this feature permits exploitation of parallel computing technologies in order to greatly improve the feasibility of treating large three-dimensional discretizations.

While the stiffness computations are relatively straightforward to implement in a parallel environment, the solution of the resulting system of equations poses a greater challenge. Since direct solvers are difficult to optimize on a parallel machine, it is advantageous to use an iterative procedure, such as the conjugate-gradient method. In this context, enforcing the incompressibility constraint requires special attention, since it degrades the numerical condition of the resulting system of equations. In the current formulation, incompressibility is enforced using a modified consistent-penalty approach, which seeks to decouple the solution for the pressure field from the conjugate-gradient method. Details of the parallel implementation of the formulation on the Intel Paragon may be found elsewhere (Sarma *et al* 1998a).

3. Results and discussion

The formulation described above has been used to simulate the deformation of single crystals of aluminium with different initial orientations, as well as polycrystalline aggregates. For the single crystal simulations, all elements of the mesh were assigned the same orientation. For the polycrystals, all elements of a grain were initialized with the orientation of that grain. Deformation corresponding to idealized plane strain compression was imposed through specification of boundary velocities. One of the sides of the parallelepiped shaped domain was assumed to be a symmetry plane and the other side was unconstrained. Nodes on the front, back and bottom faces were constrained to remain in plane. Velocities of nodes on the top surface were prescribed to maintain a constant rate of deformation. Compressive strain increments of 1% were used to model the deformation. Since the deformation approximates the conditions at the centre of a rolled sheet, the coordinate axes X , Y and Z are identified with the rolling (RD), transverse (TD) and normal directions (ND), respectively.

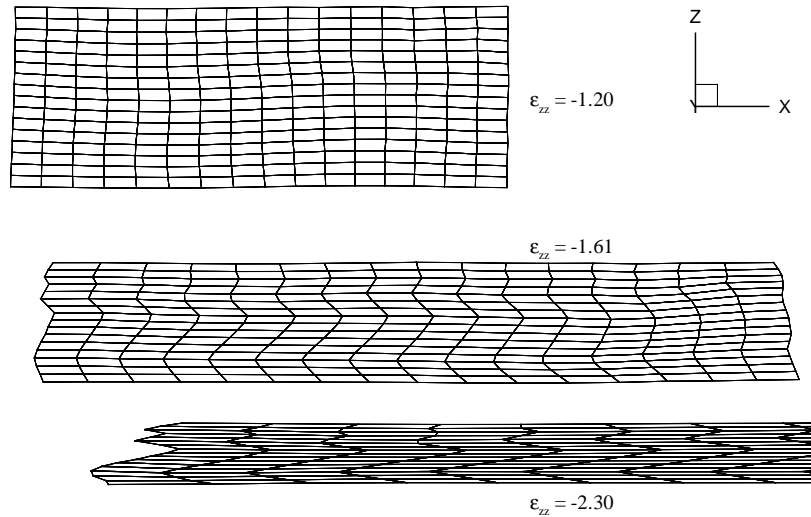
For the polycrystal deformation simulations, differences in orientations of grains lead to inhomogeneous deformation. For the single crystal simulations, since the initial orientations are the same for all elements, ideally the mesh should deform in a homogeneous fashion. However, due to small numerical differences in the element calculations which accumulate with increasing time steps, random deviations from homogeneous deformation arise. These deviations propagate with strain, eventually causing the single crystal to 'break up', depending on the orientation of the crystal. It is also possible to introduce the inhomogeneity by randomly perturbing the orientations of the elements from the perfect orientation (Becker *et al* 1991). The effect is to accelerate the development of non-uniform deformation, so that deviations are observed at smaller strain values.

3.1. Deformation of single crystal with orientation (001)[110]

The deformation of a single crystal with initial orientation (001)[110] was simulated using material parameters listed in table 1. Various experimental and modelling studies have shown this orientation to be unstable during plane strain compression, with the crystal rotating to the complementary copper components at large strains (Butler and Hu 1989, Becker *et al* 1991, Akef and Driver 1991, Cizek *et al* 1996). For this reason, this particular orientation was considered a good test case to examine the performance of the model in predicting the

Table 1. Material parameters for simulations of (001)[110] oriented single crystal.

m	$\dot{\gamma}_0$	H_0	$\hat{\tau}_i$	τ_{s0}	$\dot{\gamma}_s$	m'
0.016	0.01 s^{-1}	58.41 MPa	20.0 MPa	75.0 MPa	$5.0 \times 10^{10} \text{ s}^{-1}$	0.0

**Figure 1.** Deformed meshes of the inner 16×16 elements for section 10 (out of 20) from the 3D simulation of plane strain compression of a crystal initially oriented at (001)[110].

development of inhomogeneity in the crystal. The simulations were also used to compare the use of a 3D against a planar discretization. The 3D simulations were carried out using a mesh of $20 \times 20 \times 20$ eight-node brick elements, with initial aspect ratio of elements along X , Y and Z of 1:2:4. The deformation is uniform initially, but becomes non-uniform with increasing strain as seen from figure 1, which shows the inner 16×16 elements in the RD–ND plane from the mid-section along the TD. There is considerable RD–ND shear in opposite directions in different layers of elements. Examination of the entire 3D mesh shows that no other types of shear develop, so that material lines viewed along the RD and ND remain straight and parallel throughout the deformation. This is quite consistent with experimental observations using optical micrographs from deformation of (001)[110] oriented single crystals (Becker *et al* 1991, Akef and Driver 1991). Formation of transition bands which separate regions of opposite shear is captured by the model. In addition, the experiments reveal that these bands become high angle boundaries which run parallel to the RD and TD, as seen at high strains in the simulation results. While the formation of the shear layers is somewhat evident from the 2D simulations by Becker *et al* (1991), 3D simulations show that the high-angle boundaries separating the layers of opposite shear are indeed in the RD–TD plane.

An interesting aspect of the deformation of the (001)[110] single crystal is that it is essentially 2D in behaviour. The different sections along the TD are identical to each other in their behaviour, so that a 2D simulation is adequate to simulate the deformation. This has been verified by conducting a simulation using a 20×20 mesh of elements in the RD–ND plane, which is only one element thick along the TD. The results are identical to the 3D case, indicating that for this particular orientation there is no variation in the deformation along TD.

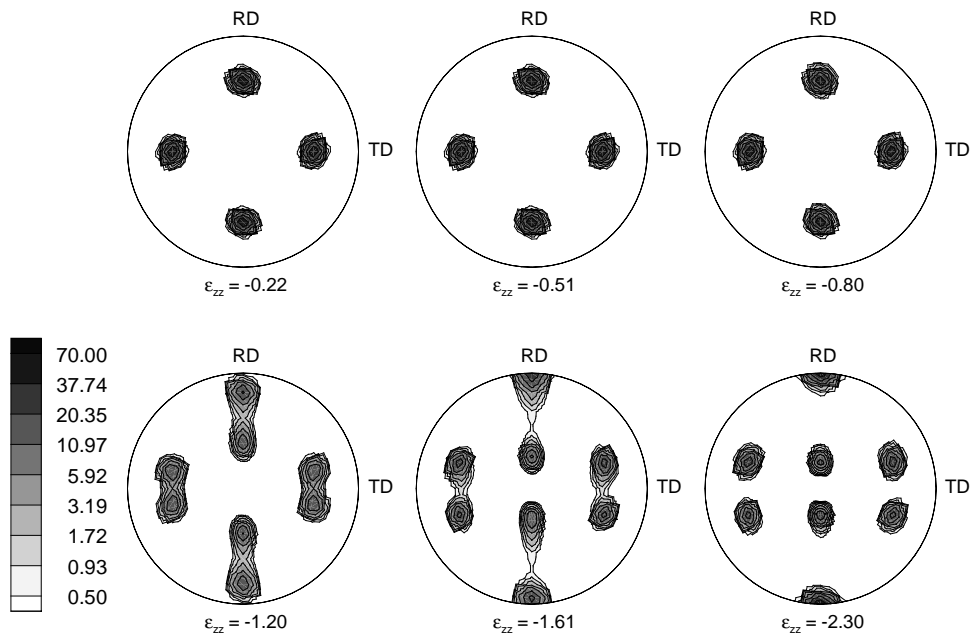


Figure 2. (111) pole figures in equal area projection showing texture evolution during plane strain compression of a crystal initially oriented at (001)[110].

The shearing causes the material to rotate in opposite directions about the TD to the two copper components, $(112)[\bar{1}\bar{1}1]$ and $(\bar{1}\bar{1}2)[\bar{1}\bar{1}\bar{1}]$. Calculation of the misorientation between the initial and final orientations of the elements indicates rotation about the [010] axis (i.e. TD) by $\pm 35^\circ$. The texture evolution is shown in figure 2 in the form of (111) pole figures, generated using popLA (Kallend *et al* 1991) assuming cubic crystal symmetry and a 5° Gaussian smoothing.

The average rotation of the lattice, computed by taking the average of the misorientation values of the inner 4096 elements with the initial (001)[110] orientation, is plotted against the compressive strain in figure 3. Similar plots are presented by both Becker *et al* (1991) and Akef and Driver (1991) to compare their models with experimental data. The data show that the lattice rotation starts at a much smaller strain compared to the value predicted by the present simulations. This is due to the assumption of a perfect crystal with all elements initially at the same orientation, which leads to a strain of about 0.7 before deviations among the elements become significant. However, if the origin is shifted appropriately, then the increase in rotation angle is quite consistent with the experimental data. The analytical expression derived by Akef and Driver predicts a faster rotation to the copper orientation than is observed from the measurements. The results of the current simulations capture quite well the decrease in rotation rate at large strains as the copper component is approached.

Simulations using a fully 3D mesh and a mesh with a single layer of elements in the RD–ND plane were also carried out for an initial orientation rotated 3.5° about ND from (001)[110]. The deviation from the symmetry of the (001)[110] orientation leads to differences between the 3D and planar meshes. As seen from figure 4, which shows the inner 16×16 elements for the planar case, the deformation is no longer restricted to XZ shear. The 3D mesh, on the other hand,

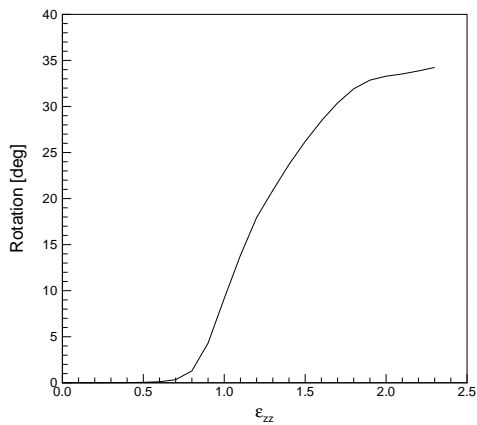


Figure 3. Variation of the average rotation of the crystal with strain, from an initial (001)[110] orientation.

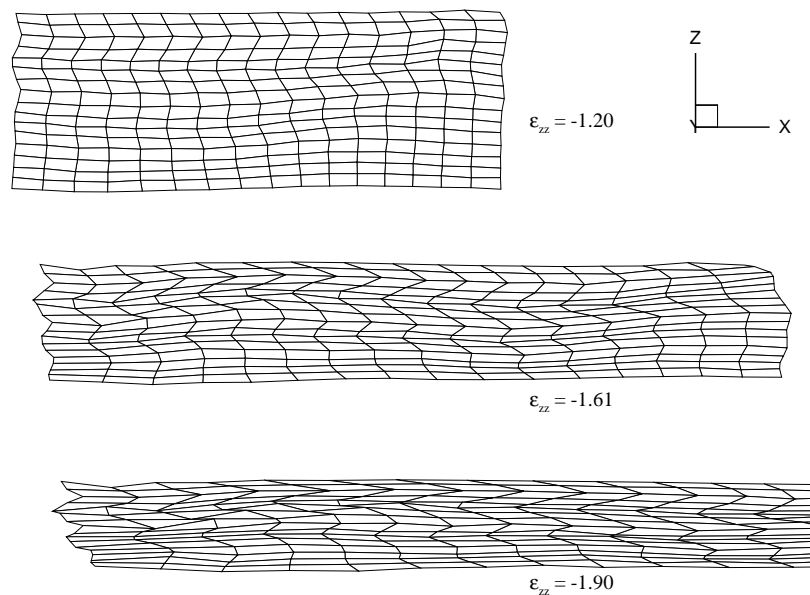


Figure 4. Deformed meshes of the inner 16×16 elements from the planar simulation of plane strain compression of a crystal initially rotated 3.5° about ND from (001)[110].

deforms more like the exact (001)[110] orientation, as shown in figure 5. The texture results reflect the influence of the deformation. The 3D simulation, with predominant XZ shear, leads to rotation about the TD towards the copper components, but with a superimposed rotation about the ND due to the initial orientation. This trend is also observed in the experimental results from channel die compression of a (001)[110] crystal initially misoriented by a 3.5° rotation about the compression axis (Becker *et al* 1991). Examination of the pole figures from the experiments shows a slight rotation about the ND, though it is not as pronounced as in the simulation results shown in figure 6. Texture results from the planar simulation are presented in figure 7. A greater amount of element shearing in different directions leads to more inhomogeneity and greater spread in the textures with lower peak intensities. These results indicate that except for special cases where symmetry between the orientation of the crystal

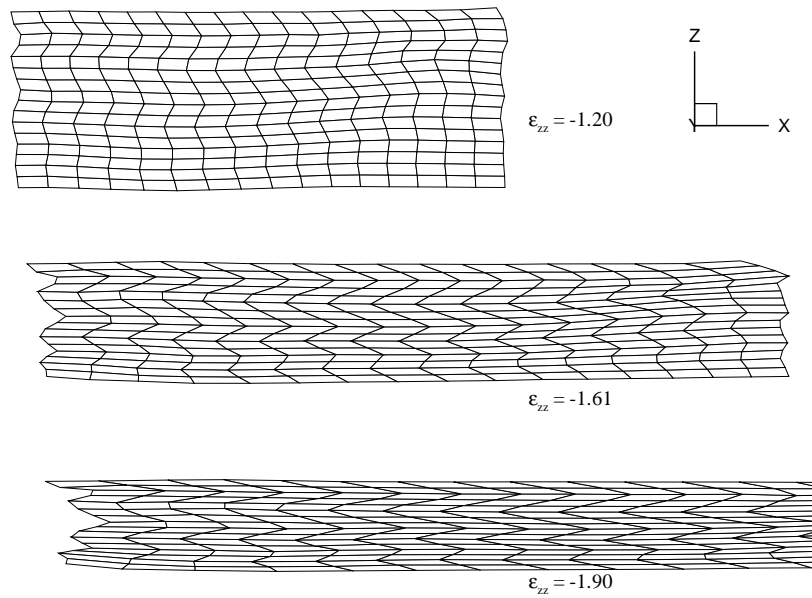


Figure 5. Deformed meshes of the inner 16×16 elements for section 10 (out of 20) from the 3D simulation of plane strain compression of a crystal initially rotated 3.5° about ND from (001)[110].

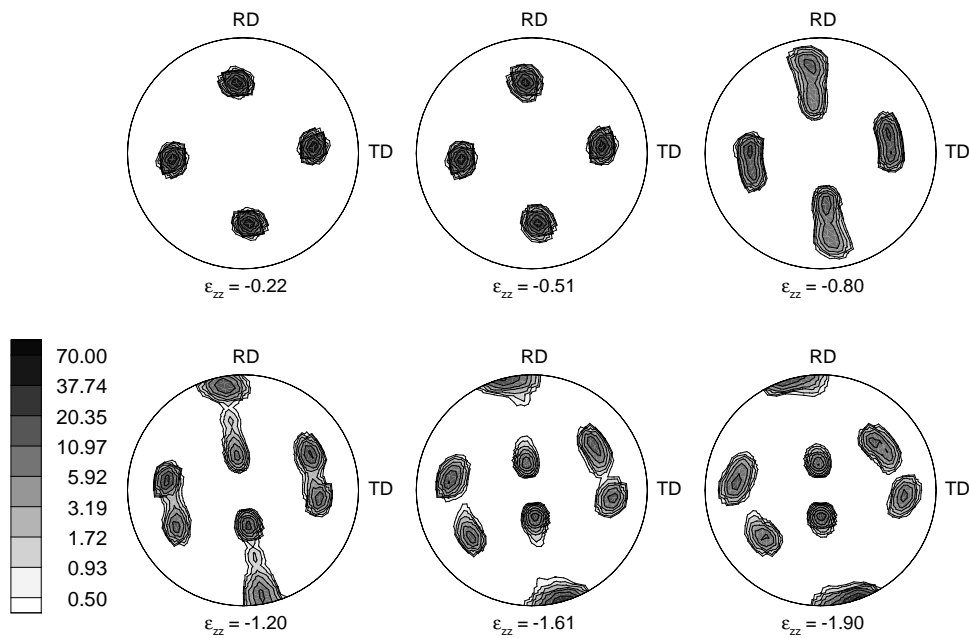


Figure 6. (111) pole figures in equal area projection showing texture evolution during plane strain compression of a crystal initially rotated 3.5° about ND from (001)[110] simulated using a 3D mesh.

and the applied deformation plays a role, constraints imposed by using only a single layer of elements or a 2D approximation can lead to considerable differences from a full 3D analysis.

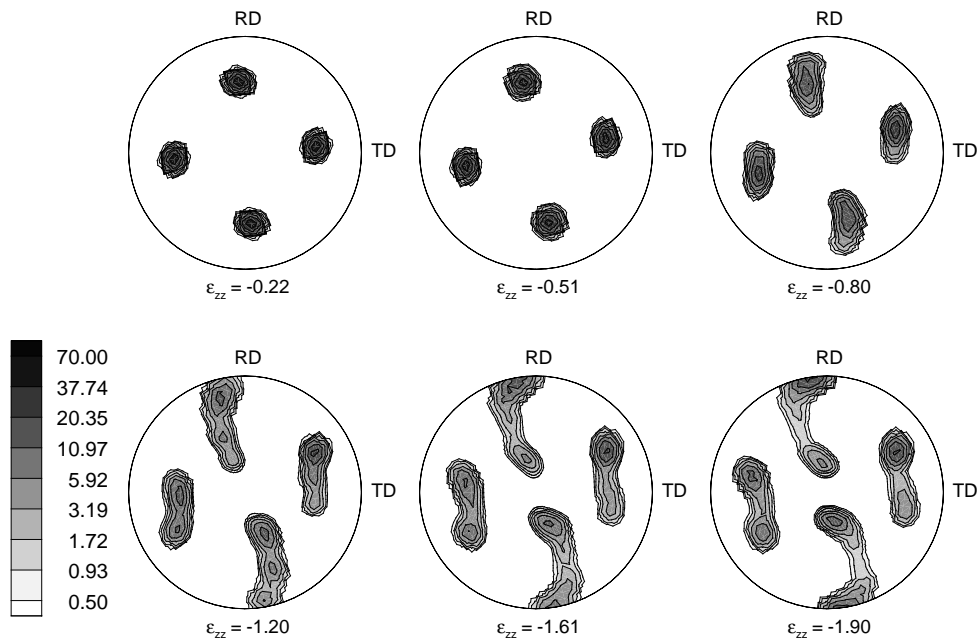


Figure 7. $\{111\}$ pole figures in equal area projection showing texture evolution during plane strain compression of a crystal initially rotated 3.5° about ND from $(001)[110]$ simulated using a planar mesh.

3.2. Effect of slip on $\{110\}$ planes in cubic single crystals

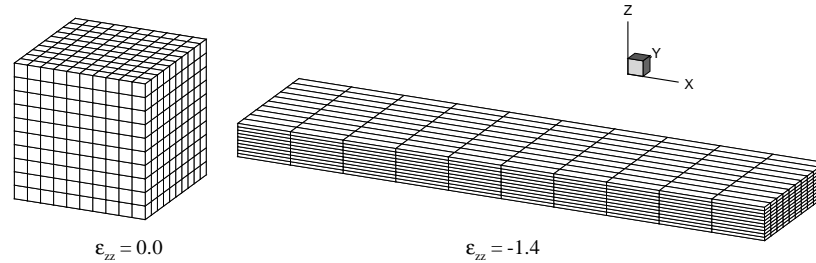
The approach discussed above for simulating the deformation of single crystals has been applied to cubic and near-cubic orientations, to study the effect of slip on $\{110\}$ planes on the stability of the cubic orientation. These simulations may be viewed as numerical experiments involving the deformation of single crystals. As mentioned earlier, previous modelling work on the effect of $\{110\}$ slip has focused on the texture evolution of an aggregate of grains, using various assumptions to relate the overall deformation to the deformation of each grain. This approach is not suited to examine the inhomogeneous deformation of individual grains. The modelling approach using FEM provides the capability to study the non-uniform deformation of single crystals, as illustrated above for $(001)[110]$ oriented crystals.

For each simulation, the crystal was discretized with 4096 elements arranged in the form of a cube with 16 elements along each side. The inner 1000 elements were used for examining the texture development. Material parameters used for the simulations, based on mechanical test data for aluminium (Mathur and Dawson 1989) are listed in table 2. Maurice and Driver (1997a) have examined the relative values of the critical resolved shear stress on the $\{111\}$ and $\{110\}$ planes, and conclude that they are almost identical at elevated temperatures. Based on their results, the critical resolved shear stress was assumed to be the same for all slip systems (for both $\{111\}$ and $\{110\}$ planes).

The deformation of a crystal at the cubic orientation $(001)[100]$ was modelled first, using the standard 12 ($\{111\}\langle 110\rangle$) slip systems. The results showed the orientation to be stable to fairly large strains, with the ability to deform in plane strain compression with no change in orientation. The initial and deformed meshes are shown in figure 8, indicating the uniform deformation of the cubic-oriented crystal. Experiments on plane strain compression

Table 2. Material parameters for the deformation simulations to study effect of slip systems.

m	$\dot{\gamma}_0$	H_0	$\hat{\tau}_i$	τ_{s0}	$\dot{\gamma}_s$	m'
0.05	1.0 s^{-1}	58.41 MPa	27.17 MPa	61.80 MPa	$5.0 \times 10^{10} \text{ s}^{-1}$	0.005

**Figure 8.** Initial and deformed meshes for the inner 1000 elements from plane strain compression of a cubic-oriented crystal using 12 slip systems.

of cubic-oriented single crystals have shown that it is not stable at low temperatures, but is at high temperatures (e.g. Maurice and Driver 1997a). Examination of the slip system activity revealed that the deformation was accommodated by equal slip on the complementary systems $(11\bar{1})[101]$, $(1\bar{1}\bar{1})[101]$, $(1\bar{1}\bar{1})[10\bar{1}]$ and $(111)[10\bar{1}]$, so that the crystal continued to deform with no rotation. Deviation from the mathematically exact cubic orientation was considered necessary to cause variations in the slip system activity, and hence development of non-uniform deformation.

The deformation of a crystal misoriented by a small amount from the exact cubic orientation was modelled without and with the six $\{110\}\langle 110\rangle$ slip systems. The initial orientation of the crystal was taken to be $(0^\circ, 5^\circ, 5^\circ)$ in terms of Euler angles using Kocks convention[†] (Kocks 1988). The choice of the amount of deviation from an exact cube was somewhat arbitrary. A somewhat large misorientation was chosen to verify the rotation of the elements towards an exact cube in the presence of $\{110\}$ slip, as indicated by some analytical results (Maurice and Driver 1993). For the simulation with 12 slip systems, the crystal initially deforms with maximum shear rates on the $(11\bar{1})[101]$ and $(1\bar{1}\bar{1})[10\bar{1}]$ systems, and with smaller shears on $(1\bar{1}\bar{1})[101]$ and $(111)[10\bar{1}]$. Some of the other slip systems also show limited activity. In the presence of the $\{110\}\langle 110\rangle$ slip systems, the maximum shear rates occur on the complementary slip systems $(101)[10\bar{1}]$ and $(10\bar{1})[101]$, with smaller values on the slip systems with the same directions on the $(11\bar{1})$ and (111) planes, respectively.

The texture evolution computed using the orientations of the inner 1000 elements is shown in figure 9 for the two cases. After a 50% reduction ($\varepsilon_{zz} = -0.7$), there is no noticeable difference between the two textures. With further deformation, the crystal deforming with 12 slip systems begins to show deviation from its initial orientation. After about 83% reduction ($\varepsilon_{zz} = -1.8$), the texture consists of two main peaks, but shows appreciable spread about them. The crystal deformed using 18 slip systems shows some inhomogeneity, but in this case the initial misorientation from cubic gradually disappears, with most of the elements rotating towards cubic orientation. The initial orientation represented by an axis and angle pair (Becker and Panchanadeeswaran 1989) has a misorientation of 7° from cubic. After deformation to $\varepsilon_{zz} = -1.8$, more than 85% of the elements are misoriented by less than 5° from cubic for the 18 slip system case, whereas with 12 slip systems that number is less than 6%.

[†] $(90^\circ, 5^\circ, 85^\circ)$ in Bunge notation.

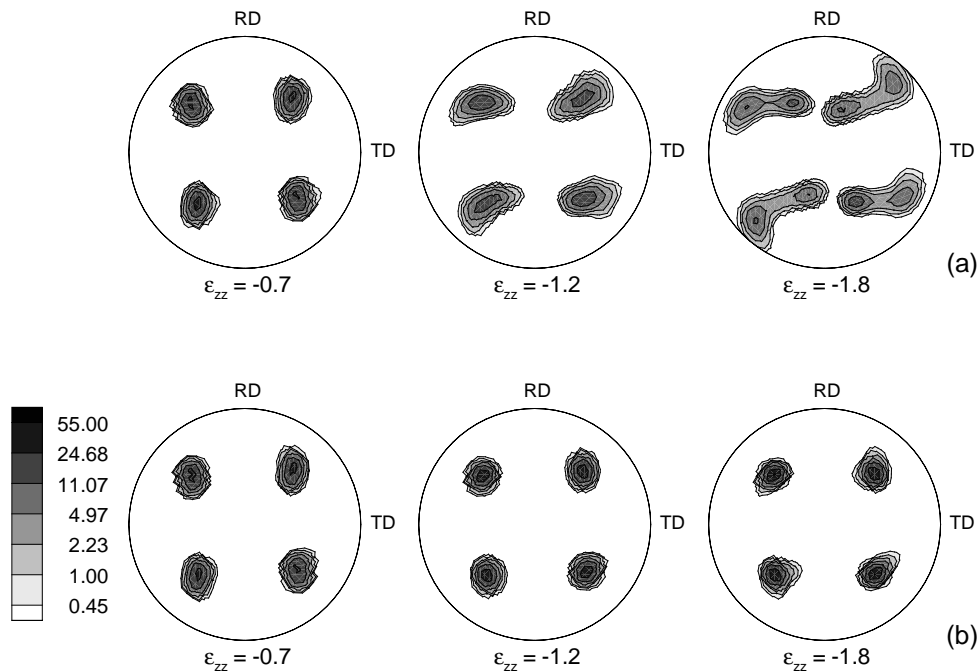


Figure 9. $\{111\}$ pole figures in equal area projection showing texture evolution of a crystal slightly misoriented from cubic, deformed in plane strain compression using (a) 12 slip systems and (b) 18 slip systems.

Examination of the slip system activity after deformation to $\varepsilon_{zz} = -1.8$ shows that in the presence of 18 slip systems almost all of the elements deform with maximum and equal shear rates on the $(101)[10\bar{1}]$ and $(10\bar{1})[101]$ systems. Only a few elements have maximum shear values on either the $(11\bar{1})[101]$ or the $(1\bar{1}1)[10\bar{1}]$ systems. These elements are also the ones with high misorientation values from cubic orientation. Thus, the effect of the presence of $\{110\}$ planes is only felt for orientations within about 14° of cubic. With increasing misorientation, the contribution of shear on the $\{110\}$ planes diminishes.

The deformed meshes for the crystal misoriented from cubic after 70% reduction are shown in figure 10 for both 12 and 18 slip systems. Both cases show significant XZ shear deformation in the same direction, and smaller degree of XY shear in opposite directions. Deformation with 12 slip systems also leads to some YZ shear, which is not as pronounced with 18 slip systems. The deformation is far more uniform with 18 slip systems, leading to the sharp cubic texture, whereas the greater inhomogeneity for the 12 slip system case leads to more diffuse texture. These results show that the addition of the $\{110\}\langle 110\rangle$ slip systems helps to stabilize the cubic orientation during plane strain compression.

3.3. Effect of slip on $\{110\}$ planes in polycrystals

In the previous subsection, the deformations of single crystals at and near cubic orientation were considered with and without $\{110\}\langle 110\rangle$ slip systems. The crystals were not influenced by the presence of neighbouring grains, as would be the case in a microstructure. In this subsection we consider the deformation of an aggregate of grains, each of which is discretized with many elements to model its non-uniform deformation in the presence of constraints from

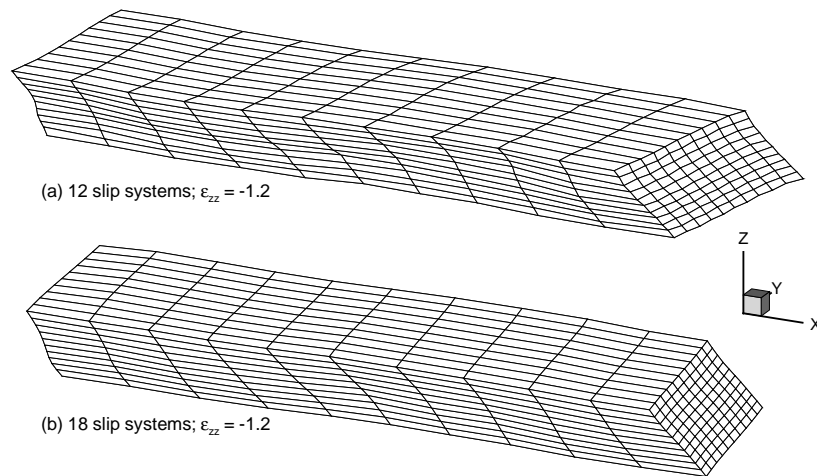


Figure 10. Deformed meshes for the inner 1000 elements from plane strain compression of a crystal slightly misoriented from cubic using (a) 12 slip systems and (b) 18 slip systems.

the surrounding grains. The simulation procedure was applied to a microstructure consisting of 53 grains (Sarma *et al* 1998b), discretized using a total of 27 000 elements arranged in a $15 \times 30 \times 60$ mesh. The initial mesh and microstructure are shown in figure 11(a), where the different colours in the microstructure indicate different grains. The initial orientations of the grains were chosen from a random sampling of Euler space, but since each grain is weighted by the number of elements used to discretize it, the initial texture is not random. The orientation of the largest grain was taken to be cubic, and the microstructure was deformed in plane strain compression to a compressive strain of $\epsilon_{zz} = 0.7$ (50% reduction in height) using 12 and 18 slip systems. The deformed mesh from the simulation using 12 slip systems is shown in figure 11(b), and depicts the inhomogeneous deformations of the grains. While the overall deformation has no shear components, the individual elements undergo shear deformations to varying extent. Introduction of additional $\{110\}$ slip planes does not lead to significant differences in the deformed mesh, indicating that for most grains (orientations), the additional slip systems do not play a major role.

Figure 12 shows the texture after 50% reduction for deformation with 12 and 18 slip systems. The pole figures were constructed from the 27 000 element orientations after applying cubic crystal symmetry and orthotropic sample symmetry. The two textures are very similar except for the peak intensity values at the cubic orientation. The other features are almost identical, resembling typical rolling texture components. The influence of the initial texture leads to a strong $\{123\}\langle 634 \rangle$ S component and a weaker $\{112\}\langle 111 \rangle$ copper component. The simulation using 18 slip systems leads to a much stronger cubic component, indicating once again the stabilizing effect of slip on $\{110\}$ planes.

While the textures as a whole are very similar, there are some variations in the individual element reorientations, with the misorientation among corresponding elements exceeding 50° in some cases. For most of the grains the difference between deformation with 12 and 18 slip systems is minor, with only a small fraction of the elements comprising the grains being misoriented by more than 10° . However, a few of the grains show significant misorientations for a large fraction of elements after deformation with 12 and 18 slip systems.

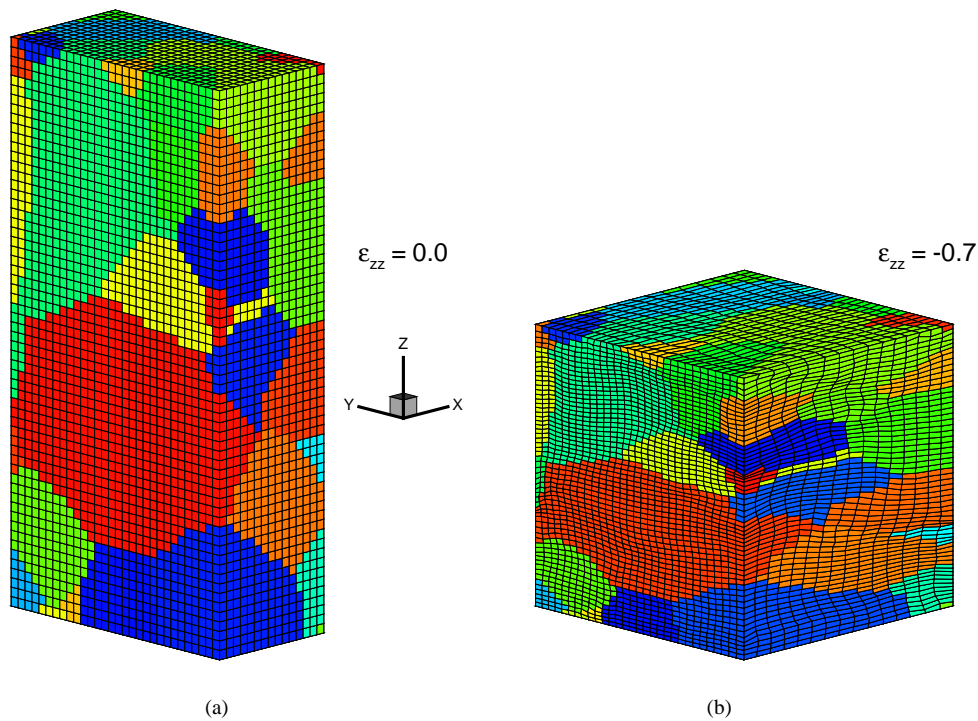


Figure 11. Initial and deformed mesh and microstructure for polycrystal simulations using 12 slip systems. (a) Discretized initial microstructure, (b) deformed microstructure.

The influence of the slip systems on the deformation of the cube-oriented grain is examined through the spread of the orientations of the elements comprising the grain after a 50% reduction. The orientations were converted from Euler angles to axis-angle pairs[†], and the resulting histogram for the distribution of angles is shown in figure 13. Since the cubic orientation coincides with the reference axes, the angle of rotation also represents the deviation from cubic. The histogram for 18 slip systems shows that most of the elements are misoriented from cubic by less than 10° , with very few elements rotating away by more than 15° . The opposite is true for the case of 12 slip systems, with a far greater number of elements misoriented by high angles. The influence of the neighbouring grains in the microstructure causes the initially cube-oriented grain to rotate away, but slip on $\{110\}$ planes retards the rate of rotation.

In the single crystal simulations of cubic and near-cubic orientations, the overall deformation of the crystal was determined by the applied boundary conditions. Therefore, most elements of the crystal were subjected to plane strain compression. However, in the case of the polycrystal, the deformation of the grain is strongly influenced by its neighbours, so that the deformation can deviate appreciably from plane strain compression, especially at regions close to the grain boundaries. In order to study the influence of the proximity to the grain boundary on the elements with initial cubic orientation, they were classified as interior or boundary elements, depending on whether the adjacent elements belonged to the same or different grains in the initial microstructure. The number of adjacent elements was varied to

[†] Cubic crystal symmetry was used to determine the symmetrically equivalent axis and angle with the smallest angle of rotation.

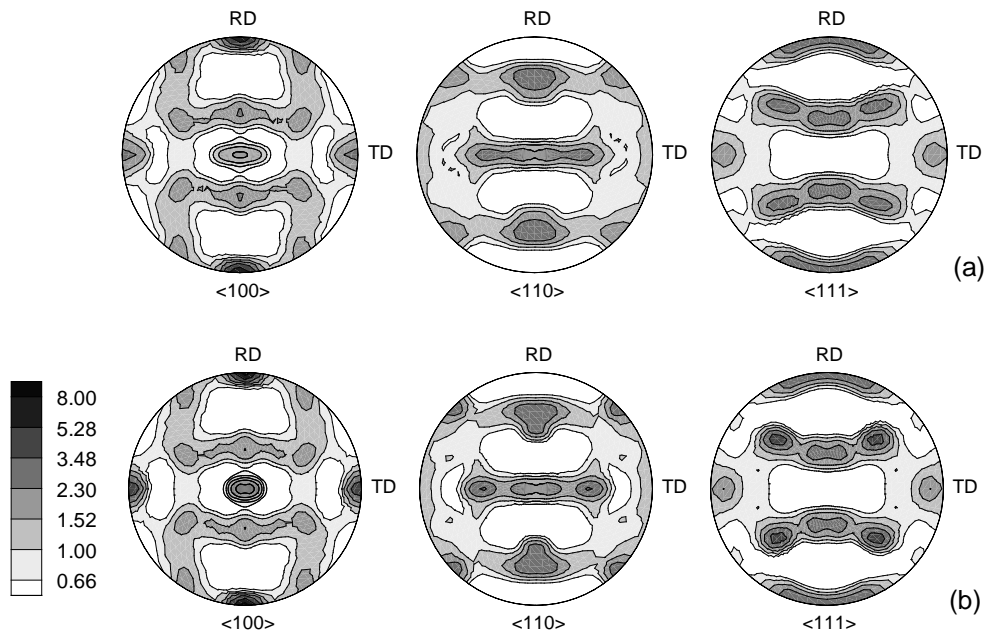


Figure 12. Pole figures in equal area projection showing the texture after deformation to $\epsilon_{zz} = -0.7$ using (a) 12 slip systems and (b) 18 slip systems for the microstructure with initial cubic grain.

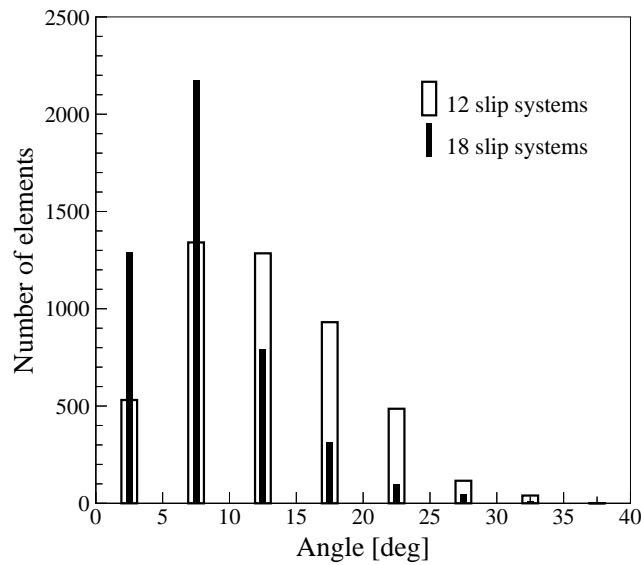


Figure 13. Histograms showing distribution of angles of rotation for the elements comprising the initially cube-oriented grain.

get sets of boundary elements of different thicknesses. Table 3 shows the comparison between the 18 and 12 slip system cases for different thickness values for the boundary elements. As the boundary thickness increases, the maximum angle of rotation for the interior elements

Table 3. Comparison of interior and boundary regions of an initially cube-oriented grain.

Thickness of boundary elements	Maximum θ among interior elements		Interior elements with $\theta < 10^\circ$ (%)		Boundary elements with $\theta < 10^\circ$ (%)	
	18 slip systems	12 slip systems	18 slip systems	12 slip systems	18 slip systems	12 slip systems
1	31.5°	34.2°	76.0	38.6	65.0	42.1
2	23.0°	30.4°	78.4	36.7	67.1	42.9
3	18.4°	28.6°	78.7	34.2	69.9	42.8
4	17.9°	27.2°	77.9	31.2	71.6	42.5

decreases for both cases. However, the decrease is far greater for 18 slip systems, with a maximum deviation from cubic of only $\approx 18^\circ$ when the boundary is four elements thick, compared to $\approx 27^\circ$ for 12 slip systems. The increase in the maximum angle from the interior to the boundary indicates the effect of neighbouring grains on the deformation. The elements near the boundary have greater deviations from plane strain deformation compared to elements in the grain interior, and as a consequence, may be expected to be less affected by the stabilizing presence of the $\{110\}$ slip systems.

Another indication of the difference between 12 and 18 slip systems comes from the examination of the percentage of interior and boundary elements that remain close to cubic after deformation. As seen from table 3, the fraction of elements which rotate by less than 10° away from initial cubic is greater for 18 slip systems for both interior and boundary elements. The fraction of interior elements with small misorientation from cubic remains close to 78% with different boundary thickness values. The fraction of boundary elements with $\theta < 10^\circ$ goes down as the boundary thickness reduces, indicating the increasing effect of neighbouring grains as one gets closer to the boundary. The heterogeneity in deformation also makes the $\{110\}$ slip systems less effective than in the case of more homogeneous plane strain deformation conditions.

The boundary effect is also seen for the case of 12 slip systems, although the trend is reversed. As the boundary thickness increases, causing fewer elements to be considered as part of the interior, the fraction of interior elements with small misorientation from cubic decreases. This means that as one goes towards the interior of the grain, one finds fewer grains with small misorientation from cubic. Near the boundary, the effect of neighbouring grains is in fact to retard the rotation away from cubic, so that the fraction of boundary elements with small misorientation from cubic remains fairly constant.

It must be mentioned here that the results presented on the boundary and interior elements are intended to highlight the differences between the absence and presence of $\{110\}$ slip planes on the cubic grain, and these results are insufficient to draw conclusions regarding the size of the zone of influence near the grain boundaries. Determining the zone of influence would require additional simulations to ensure that mesh resolution effects are accounted for, which is beyond the scope of this work. Even if such simulations are performed, the zone of influence can only be determined relative to the grain size and not as an absolute measure, since there is no size scale implicit in the model.

Simulations without and with the $\{110\}\langle 110 \rangle$ slip systems were also carried out using the 3D microstructure where there was no initial cubic grain. In this case, there was no appreciable difference between the two resulting textures as a whole, leading to typical rolling components (Sarma *et al* 1998b). However, when individual grains were examined, a few of them showed significant differences either due to their location or their orientation. The presence of the

initial cubic grain leads to some differences in the reorientation of individual elements of various grains, but the deformations are by and large quite similar. This indicates that slip on $\{110\}$ planes is only significant for select orientations such as the cubic orientation, and is not a factor for most of the other orientations.

Finally, it must be mentioned that for the deformation of the single crystal near cubic, only at fairly large strains is there an appreciable difference in textures between 12 and 18 slip systems (figure 9). However, for the case of a polycrystal, a 50% reduction is enough to bring about significant differences between deformation with 12 and 18 slip systems. This is another indication of the effect of grain interactions, which lead to a more heterogeneous deformation state in the microstructure compared to the more homogeneous conditions of plane strain compression in the single crystal.

4. Summary and conclusions

The combination of crystal plasticity and the FEM provides a powerful approach for simulating the deformation of metals at the mesoscale. By discretizing individual grains, the method allows for modelling the deviations from applied overall deformation, not only from grain to grain but also within the individual grains. The non-uniform deformations of individual grains and their interactions with neighbours can be accounted for using this approach. The methodology has been applied to study deformations of single crystals and polycrystals of aluminium, and to examine the effect of including slip on $\{110\}\langle 110\rangle$ systems. Unlike prior modelling efforts using aggregates of grain orientations, the present approach does not require assumptions to partition the applied deformation among the grains, and is hence suitable to study even single crystal deformations.

Simulations with $(001)[110]$ oriented crystals were used to show the ability of the formulation to model the development of shears in the RD–ND plane and the consequent rotation of the crystal about TD to the copper orientation, as has been observed in plane strain compression experiments. These simulations also show that due to symmetry of the crystal with respect to the applied deformation, the $(001)[110]$ orientation deforms with only RD–ND shear. However, a slight rotation from the exact $(001)[110]$ orientation leads to development of other localized shears, so that 2D and 3D simulations no longer lead to the same result.

Simulations with single crystals initially at orientations close to cubic show that slip on $\{110\}$ planes stabilizes the cubic orientation, with the crystal rotating towards the cube during plane strain compression. The same trend is also observed in a cube-oriented crystal which is part of a larger polycrystalline aggregate. The results presented here are in good agreement with experimental data on hot deformed aluminium alloys. In particular, slip on $\{110\}$ planes favouring stability of cube-oriented grains has been observed in both single crystals and polycrystals. The addition of $\{110\}$ planes does not radically change the overall texture, but merely improves the strength of the cubic component. This would indicate that the effect of the $\{110\}$ slip planes is restricted to a few special orientations like cubic. The influence of neighbour constraints is also evident from the polycrystal simulations. Elements close to grain boundaries are affected to a greater extent by the neighbouring grains, leading to greater deviation from plane strain deformation and a smaller influence of the $\{110\}$ planes.

Due to the difficulty in performing experiments with a small aggregate of grains and monitoring all the grains throughout the deformation process, it is not easy to compare the polycrystal simulations directly with experiments. On the other hand, it is also not trivial to carry out such detailed simulations at the mesoscale with large numbers of grains. Therefore, it becomes necessary to perform the comparisons with single crystal experiments. That is one reason for the simulations with the cubic crystals and with the $(001)[110]$ oriented crystal,

which has been the focus of several experiments. The crystal with slight misorientation from cubic when deformed with the usual octahedral slip systems rotates away to other orientations. Various experiments with cubic crystals at room temperature have shown that it is not stable, and its reorientation is quite complex and not restricted to rotation about a particular axis. The simulations also show that different elements rotate about different axes, and that the final texture is somewhat diffuse. The choice of the initial orientation may be expected to play a role in the texture evolution, and further study is required to determine the reorientation path for near-cubic orientations.

Based on observations of slip traces in single crystals deformed in plane strain compression at elevated temperatures, Maurice and Driver (1997a) conclude that non-octahedral slip systems are active at higher temperatures. The results of their numerical simulations (Maurice and Driver 1997b) show that addition of $\{112\}$, $\{110\}$ and $\{001\}$ slip planes leads to increased strength of certain texture components such as brass and cubic, as commonly observed in hot rolled aluminium alloys. The results of the present simulations would indicate that specific non-octahedral slip systems favour stability of specific orientations. The introduction of these additional slip systems offers one possible means to apply the mesoscale modelling approach to hot deformation of aluminium alloys and other fcc metals.

Acknowledgments

This research was sponsored by the Office of Basic Energy Sciences, US Department of Energy, under contract DE-AC05-96OR22464 with the Lockheed Martin Energy Research Corporation. The research was supported in part by an appointment to the Oak Ridge National Laboratory Postdoctoral Research Associates Program administered jointly by the Oak Ridge National Laboratory and the Oak Ridge Institute for Science and Education. The authors acknowledge the use of the Intel Paragon XP/S 35 computer, located in the Oak Ridge National Laboratory Center for Computational Sciences (CCS), funded by the Department of Energy's Mathematical, Information, and Computational Sciences (MICS) Division of the Office of Computational and Technology Research.

References

- Akef A and Driver J H 1991 *Mater. Sci. Engng A* **132** 245–55
 Anand L and Kalidindi S R 1994 *Mech. Mater.* **17** 223–43
 Bacroix B and Jonas J J 1988 *Textures Microstruct.* **8/9** 267–311
 Beaudoin A J, Dawson P R, Mathur K K and Kocks U F 1995 *Int. J. Plast.* **11** 501–21
 Beaudoin A J, Dawson P R, Mathur K K, Kocks U F and Korzekwa D A 1994 *Comput. Methods Appl. Mech. Engng* **117** 49–70
 Beaudoin A J Jr, Mecking H and Kocks U F 1996 *Phil. Mag. A* **73** 1503–17
 Becker R 1991 *Acta Metall.* **39** 1211–30
 Becker R, Butler J F Jr, Hu H and Lalli L A 1991 *Met. Trans. A* **22** 45–58
 Becker R and Panchanadeeswaran S 1989 *Textures Microstruct.* **10** 167–94
 ——— 1995 *Acta Mater.* **43** 2701–19
 Butler J F Jr and Hu H 1989 *Mater. Sci. Engng A* **114** L29–33
 Cizek P, Wynne B P, Lu H and Parker B A 1996 *Mater. Sci. Engng A* **219** 44–55
 Honneff H and Mecking H 1978 *Proc. Fifth Int. Conf. on Textures of Materials (ICOTOM 5)* ed G Gottstein and K Lücke (Berlin: Springer) pp 265–75
 Kalidindi S R, Bronkhorst C A and Anand L 1992 *J. Mech. Phys. Solids* **40** 537–69
 Kallend J S, Kocks U F, Rollett A D and Wenk H-R 1991 *Mater. Sci. Engng A* **132** 1–11
 Kocks U F 1988 *Proc. Eighth Int. Conf. on Textures of Materials (ICOTOM 8)* ed J S Kallend and G Gottstein (Warrendale, PA: The Metallurgical Society) pp 31–6
 Lebensohn R A and Tomé C N 1993 *Acta Metall. Mater.* **41** 2611–24

- Mathur K K and Dawson P R 1989 *Int. J. Plast.* **5** 67–94
Mathur K K, Dawson P R and Kocks U F 1990 *Mech. Mater.* **10** 183–202
Maurice C I and Driver J H 1993 *Acta Mater.* **41** 1653–64
———1997a *Acta Mater.* **45** 4627–38
———1997b *Acta Mater.* **45** 4639–49
Mika D P and Dawson P R 1998 *Mater. Sci. Engng A* **257** 62–76
Molinari A and Tóth L S 1994 *Acta Metall. Mater.* **42** 2453–8
Raabe D 1995 *Acta Metall. Mater.* **43** 1023–8
Radhakrishnan B, Sarma G B and Zacharia T 1998a *Acta Mater.* **46** 4415–33
———1998b *Scr. Mater.* **39** 1639–45
Sarma G, Zacharia T and Miles D 1998a *Comput. Math. Appl.* **35** 41–57
Sarma G B, Radhakrishnan B and Zacharia T 1998b *Comput. Mater. Sci.* **12** 105–23
Taylor G I 1938 *J. Inst. Metals* **62** 307–24